Heat Transfer During Freeze-Drying Using a High-throughput vial System in view of Process Scale-up to Serum vials

Juan Patricio Buceta, Ioan Trelea, Bernadette Scutellà, Erwan Bourlés, Fernanda Fonseca, Stephanie Passot

Heat transfer during freeze-drying using a high-throughput vial system in view of process scale-up to serum vials

Juan Patricio Buceta[1], Ioan CristianTrelea[1], Bernadette Scutellà[2], Erwan Bourlés[2],

Fernanda Fonseca[1], Stéphanie Passot[1]

[1] Université Paris-Saclay, INRAE, AgroParisTech, UMR SayFood, F-78850, Thiverval-Grignon, France

[2] GSK, Rixensart, Belgium

Abstract

Specific devices that combine 96-well plates and high-throughput vials were recently proposed to improve the efficiency of formulation screening. Such devices make it possible to increase the number of formulations tested while reducing the amount of active ingredients needed. The geometry of the product container influences the heat and mass transfer during freeze-drying, impacting product temperature (T_p) and therefore affecting the final product quality. Our study aimed to develop a tool to identify the operating conditions resulting in the same T_p when using high-throughput vials inside well plates and serum vials. Heat transfer coefficients between the shelf and the high-throughput vials (K_V) were measured using the gravimetric method at chamber pressures ranging from 4 to 65 Pa for a batch of 576 vials located at the centre of the well plates. K_V distributions were used to predict T_P distributions during primary drying of a 5% sucrose solution. T_p values were in average 8 °C higher using high-throughput vials instead of serum vials at chamber pressures lower than 12 Pa. This study provides a graphical solution for the management of process scale-up and scale-down between both types of product containers depending on their respective K_V and product resistance to mass transfer.

Abbreviations

Latin alphabet

A	Heat transfer area	m^2
A^C	Vial contact area	m^2
A_{in}	Inner bottom area of the vial	m^2
d_{gas}	Molecular diameter of the trapped gas	m
F	Visualisation factor	Dimensionless
K	Heat transfer coefficient	$W.m^{-2}.K^{-1}$
k	Empirical constant of proportionality	$W.m^{-4}.K^{-1}$
l	Gas layer thickness	m
l_{ice}	Ice layer thickness	m
$\dot{m}$	Sublimation mass flow leaving the container	$kg.s^{-1}$
P	Pressure	Pa
P_C	Pressure inside the chamber	Pa
P_{sat}	Ice-vapour equilibrium pressure	Pa
$\dot{Q}$	Heat flow	W
R	Ideal gas constant	$J.K^{-1}.mol^{-1}$
R_P	Product resistance per unit area	$Pa.s.m^2.kg^{-1}$
T	Temperature	K
T_b	Temperature at the bottom of the vial	K
T_p	Product temperature	K
T_{sat}	Ice-vapour equilibrium temperature	K
T_{shelf}	Shelf temperature	K
T_{WP}	Well plate temperature	K

Greek alphabet

α	Thermal accommodation coefficient for gas conduction	Dimensionless
ΔH_{sub}	Mass latent heat of sublimation	$J.kg^{-1}$
$\widetilde{\Delta H_{sub}}$	Molar latent heat of sublimation	$J.mol^{-1}$
ε	Emissivity	Dimensionless
λ_{gas}^{cont}	Gas thermal conductivity in a continuous regime	$W.m^{-1}.K^{-1}$
λ_{ice}	Thermal conductivity of the ice	$W.m^{-1}.K^{-1}$
Λ_0	Free molecular heat conductivity of the gas at 0 °C	$W.m^{-1}.K^{-1}.Pa^{-1}$
σ	Stephan-Boltzmann constant	$W.m^{-2}.K^{-4}$

Superscript

cc	Contact conduction contribution	

gc	Gas conduction contribution
HT	Refers to high-throughput vials and well plate system
rad	Radiation contribution
ser	Refers to serum vials
V	Refers to the heat transfer between the shelf and the vial bottom

Subscript

HV	Refers to high-throughput vials
t	Refers to the triple point
ser	Refers to serum vials
WP	Refers to well plates

Introduction

Freeze-drying is a dehydration method widely used in the pharmaceutical industry to preserve proteins, hormones, vaccines and bacteria, among others (Fonseca et al., 2015; Pikal et al., 1991; Pikal, 1994; Scutellà et al., 2017a). This method consists of three steps: freezing the product, removing the ice by sublimation (primary drying), and desorbing the bound water (secondary drying). Freeze-drying vaccines extends their shelf life during storage and transportation, and is the recommended procedure for formulations that are not stable enough in liquid form. Because of the rapid growth of the biopharmaceutical industry, it is necessary to find ways to accelerate the development phase of new products. Novel devices combining 96-well plates and small glass tubular containers – known as high-throughput vials – could speed-up the formulation development step by increasing the number of formulations tested per freeze-drying cycle, while limiting the amount of active ingredients. The final product containers used for commercial distribution are usually serum vials, which have a vial bottom area three times greater than high-throughput vials, and are directly placed on the freeze dryer shelf usually contained by a bottomless tray.

The US Food and Drug Administration (FDA) now requires that product quality be integrated into process design. This initiative is known as Quality by Design (QbD). Constructing a “design space” is a key step in the QbD initiative. A design space is defined as the “multidimensional combination and interaction of input variables (e.g., material attributes) and process parameters that have been demonstrated to provide assurance of quality” (US Food and Drug Administration, 2009). When considering the primary drying step of the freeze-drying process, the design space is a graphical solution of the heat and mass transfer equations, capable of predicting the product temperature and sublimation rate at a given time during the process. The design space is built taking account of the product container used at the production scale. Changing the product container during the formulation development step implies a change in the heat and mass transfer properties (Pikal et al., 1984; Pisano et al., 2011) and, consequently, the design space. The design spaces using high-throughput and serum vials must be connected in order to “translate” the results of high-throughput formulation screening to a pilot or industrial scale. This strategy enables researchers to accelerate the development of new products, particularly when the container used at industrial scale is defined and known before the formulation development step – 3 mL serum vials in our case of study. In this work, the connection between design spaces will be done considering the predicted product temperature for each vial geometry. Product

temperature is a crucial process parameter that affects product appearance; and that could subsequently result in unacceptable values of residual moisture content and reconstitution time, as well as a loss of product potency. If the product exceeds a critical temperature known as the collapse temperature, it will not present the desired appearance and will therefore not be accepted on the basis of quality standards. We will use the term “scale-up” to refer to the “translation” of the operating conditions that use high-throughput vials to the operating conditions that use serum vials at the same product temperature. Similarly, we will use the term “scale-down” for the “translation” of the operating conditions from serum to high-throughput vials.

Little research has been conducted on the heat transfer during primary drying using high-throughput vials in well plates: Patel and Pikal (2011) and von Graberg (2011) estimated a global heat transfer coefficient between the shelf and the high-throughput vial bottom (K_V), and Trnka et al. (2015) measured the temperature of plastic well plates and compared it to that of serum vials for only one set of operating conditions. In our study, we applied the approach of Scutellà et al. (2017a) for investigating heat transfer in serum vials to the high-throughput vial system. Our objective was to propose a graphical solution for interconnecting the design space of both types of product containers. Only vials located in the centre of the well plate and surrounded by other vials were considered. Different types of well plates and high-throughput vials were investigated. The global heat transfer coefficient between the shelf and the high-throughput vial bottom (K_V) was experimentally determined and was described as the contribution of two heat transfer coefficients: one between the shelf and the well plate, and one between the well plate and the vial. K_V heterogeneity was also quantified and explained by the contact area between the high-throughput vial bottom and the well plate. K_V values were used to predict the product temperature during primary drying of an aqueous sucrose solution (5% w/w). Our data on high-throughput vials were systematically compared to the data obtained with serum vials by Scutellà et al. (2017a). Finally, a graphical method was presented to scale-up and scale-down the operating conditions of the process when changing the product container.

Materials and methods

High-throughput vial system

The *96-Well Freeze-Drying System* manufactured by VirTis (SP Scientific, Stone Ridge, New York, USA) consisting of aluminium well plates and glass tubular vials, and referred to below as high-throughput vials, was used in our study. Figure 1a presents the two types of well plates used, which differ in their surface finish: (*i)* brilliant black (A-type well plate), and (*ii)* matte black (B-type well plate). A-type well plate bottom surfaces have circular marks due to the way they are manufactured, whereas B-type well plate bottom surfaces do not present such marks (Figure 1c). Furthermore, Figure 1b shows the two high-throughput vial sizes used that differ only in height, which, therefore, present a maximal filling volume of either 500-µL or 1000-µL. Figure 1b also shows a 3-mL serum vial, the traditional container used for vaccine freeze-drying (Brülls and Rasmuson, 2002; Pikal et al., 1984; Pisano et al., 2011; Scutellà et al., 2017a) for comparison. Seven A-type well plates, five B-type well plates, and 576 high-throughput vials of each size were used for the study.

A robotic tube handler (model XL9; BioMicrolab, Concord, CA, USA) shown in Figure 1d was used to weigh the high-throughput vials. The tube handler consisted of a mechanical arm and an analytical scale (± 0.0001 g). Vials were manually placed in a custom-made plate designed to fit on the loading area of the robot. The mechanical arm took the vials one by one, placed them on the analytical scale, and returned them to the custom-made plate.

Freeze dryer

A laboratory-scale freeze dryer (Epsilon 2-25D, Martin Christ Gefriertrocknungsanlagen GmbH, Osterode am Harz, Germany) was used in this study. The freeze dryer had seven shelves measuring 0.27 m^2 each, a distance between shelves of 57 mm, a drying chamber volume of 0.38 m^3, a duct between the chamber and the condenser closed by a mushroom valve, and a capacitance manometer to monitor the pressure inside the chamber. Tempris wireless temperature probes (iQ-mobil solution GMbH, Holwkirchen, Germany) were used to register the ice temperature.

Ice sublimation experiments

Ice sublimation experiments were performed using well plates with and without high-throughput vials inside. The procedure previously described by Scutellà et al. (2017a) for serum vials was applied with some modifications. Stoppers were not inserted into the vial necks.

The 1000-µL vials were filled with 600 µL of distilled water. Three A-type well plates and three B-type well plates, each filled with 96 1000-µL vials, were placed on the middle shelf of the freeze dryer according to the arrangement shown in Figure *2*a. During each experiment, the same vial was placed in the same well of the same well plate, and the same well plate was placed in the same position on the shelf. Well plates were quickly loaded onto the pre-cooled shelf at -50 °C. Relative air humidity was limited by a dry air laminar flow in front of the freeze dryer door, reducing condensation on the shelves. A freezing step of 2 hours was carried out to ensure complete water solidification. The sublimation step began after the freezing step by decreasing the chamber pressure and increasing the shelf temperature at a rate of 1 °C.min^{-1}. Experiments were carried out at 4, 6, 12, 25, and 65 Pa with a shelf fluid inlet temperature (shelf temperature) of -15 °C. Sublimation lasted long enough to remove approximately 20% of the initial ice mass. Tempris probes were inserted into three vials located in the centre of A-type well plates.

During experiments with 500-µL vials, well plates were arranged as shown in Figure *2*b, and Tempris probes were not used since they could not be properly placed in the vials. Four A-type well plates and two B-type well plates were each charged with 96 500-µL vials filled with 400 µL of distilled water.

During experiments without vials, well plates were arranged as in Figure *2*a, and one Tempris probe was placed in a well in the centre of each well plate. Well plates were filled with 60 mL of distilled water.

The time-averaged sublimation mass flow was gravimetrically measured for each vial, $\dot{m}_{HV}$, kg.s^{-1} (experiments with vials), and for each well plate, $\dot{m}_{WP}$, kg.s^{-1} (experiments without vials). $\dot{m}_{HV}$ and $\dot{m}_{WP}$ were calculated as the mass loss divided by the time the sublimation lasted. Vials of 500 µL and 1000 µL were individually weighed before and after the experiment using a robotic tube handler. The mass loss during waiting and weighing times was quantified and shown to be negligible (< 0.5% of the initial ice mass). Well plates were weighed on a precision scale (± 0.001 g; Mettler Toledo, Zaventem, 142 Belgium). Sublimation time was considered to begin when the shelf fluid inlet temperature was greater than the ice-vapour equilibrium temperature at the chamber pressure.

Measurement of dimensions and emissivity of well plates and high-throughput vials

The dimensions of 96 vials of each size (500-µL and 1000-µL), and one well plate were measured by Precis&Mans (Le Mans, Pays de la Loire, France). The following geometrical parameters were determined with a precision of 0.01 mm: (*i)* inner and outer bottom diameters of the vial; (*ii)* maximum and minimum vial bottom concavity; (*iii)* length and width of the well plate; and (*iv)* diameter and depth of the wells. These values were used to calculate additional dimensions: (*i)* inner and outer bottom areas of the vial; and (*ii)* well plate bottom area.

Emissivity measurements of the well plate surfaces and the high-throughput vials were carried out by Themacs Ingénierie (Champs sur Marne, France) using a Fourier Transform Infrared Spectrometer Frontier (PerkinElmer, Waltham, MA, USA). The emissivity of well plates and vials varied less than 0.02 between -40 °C and -10 °C; for our purposes, the emissivity values were considered to be constant and equal to the temperature-averaged values.

Furthermore, the imprint method proposed by Kuu et al. (2009) was used to evaluate the vial bottom-well plate contact area (A_{HV}^{C}) of 96 vials. This method consisted of placing the vials on an inkpad and then on a piece of white paper. The ink marks left on the paper were scanned and pixels with ink were counted using a code especially developed for this task using MATLAB R2017a (The MathWorks, Inc, Natick, MA, USA). Finally, the number of pixels per mm^2 was established using a figure of known area treated by the same procedure. The measured dimensions and surface emissivity values are given in Table 1.

Characterisation of the bottom surface of the well plate in contact with the freeze dryer shelf

The surface of A-type and B-type well plates in contact with the shelf was characterised by detailed inspection through high-definition photography. Two A-type and two B-type well plates were placed in a light-controlled cabin and were photographed using a Reflex Canon EOS camera (Canon France, Paris, France). The image of each well plate bottom surface contained 4892 × 3294 pixels. Pictures were treated using Adobe Photoshop (Adobe Inc., San José, CA, USA), original images were enlarged four times, and contrast was increased by 75% to enhance the shades created by the surface marks as presented in Figure 1c.

Numerical calculations and statistical analysis

Calculations were performed using MATLAB R2017a. The system of equations described in the section *Theory and data analysis* was solved by an iterative code especially developed for this study, and the convergence criterion was the relative tolerance of the heat flow value (0.1%). Parameter estimations were performed using the *nlinfit* function of the Statistics and Machine Learning Toolbox, chi-square goodness-of-fit tests were performed using the *chi2gof* function, and artificial standard distributions consisting of 1000 elements were created using the *normrnd* function.

Theory and data analysis

Evaluation of the heat transfer coefficients based on experimental data

By analogy with the work on serum vials (Pikal et al., 1984; Pikal, 2000; Pisano et al., 2011; Scutellà et al., 2017a), an apparent heat transfer coefficient between the shelf and the high-throughput vial bottom (K_V, W.m^{-2}.K^{-1}) was calculated using the equation:

$$K_V = \frac{\dot{Q}_{HV}}{A_{HV}\left(T_{shelf} - T_b\right)} = \frac{\dot{m}_{HV}\Delta H_{sub}}{A_{HV}\left(T_{shelf} - T_b\right)} \quad (1)$$

where $\dot{Q}_{HV}$ (W) is the heat flow received by the vial, A_{HV} (m^2) is the outer bottom area of the vial, T_{shelf} (K) is the average temperature between the inlet and outlet shelf fluid temperatures, T_b (K) is the product temperature at the bottom of the vial, ΔH_{sub} (J.kg^{-1}) is the latent heat of sublimation, and $\dot{m}_{HV}$ is the sublimation mass flow (kg.s^{-1}). Since it was not possible to insert temperature probes in all vials to monitor the product temperature at the bottom of the vial, T_b was theoretically calculated for each vial as follows:

$$T_b = T_{sat} + \frac{\dot{Q}_{HV} l_{ice}}{\lambda_{ice} A_{in}} \quad (2)$$

where λ_{ice} (W.m^{-1}.K^{-1}) is the thermal conductivity of the ice, l_{ice} (m) is the average between the initial and final ice thickness calculated based on the mass loss, A_{in} (m^2) is the inner bottom area of the vial, and T_{sat} (K) is the ice-vapour equilibrium temperature. T_{sat} was obtained using the Clausius Clapeyron relation (Perry and Green, 2008):

$$T_{sat} = \frac{T_t}{1 - \frac{RT_t}{\widetilde{\Delta H_{sub}}} ln\left(\frac{P_{sat}}{P_t}\right)} \quad (3)$$

where T_t (273.16 K) is the triple point temperature of water, P_t (611.66 Pa) is the triple point pressure of water, R (8.3144 J.K^{-1}.mol^{-1}) is the ideal gas constant, $\widetilde{\Delta H_{sub}}$ (5.1059×10^4 J.mol^{-1}) is the molar latent heat of sublimation, and P_{sat} (Pa) is the pressure at the ice sublimation front (ice-vapour interface). P_{sat} was assumed to be equal to the chamber pressure (P_C) during ice sublimation experiments, considering that: (*i)* the chamber was saturated with vapour; and (*ii)* the pressure loss between the ice sublimation front and the chamber was negligible since no stoppers were inserted into the vial necks. The calculated T_b were compared to the product temperature value registered by the Tempris probes in three 1000-µL vials, a good agreement (< 0.8 °C difference) was observed between experimental data and calculated values.

Due to the presence of the well plate between the shelf and the high-throughput vial, this apparent heat transfer coefficient K_V can be considered as a combination of two heat transfer coefficients: (*i)* a coefficient between the shelf and the well plate K_{WP}; and (*ii)* a coefficient between the well plate and the bottom of the vial K_{HV}.

K_{WP} was obtained using the data from the experiments performed without vials inside the well plates:

$$K_{WP} = \frac{\dot{Q}_{WP}}{A_{WP}\left(T_{shelf} - T_{WP}\right)} = \frac{\dot{m}_{WP}\Delta H_{sub}}{A_{WP}\left(T_{shelf} - T_{WP}\right)} \quad (4)$$

where $\dot{Q}_{WP}$ (W) is the heat flow received by the well plate, A_{WP} (m²) is the bottom area of the well plate, T_{WP} is the product temperature at the bottom of the wells (K), and $\dot{m}_{WP}$ is the sublimation mass flow of each well plate (kg.s^{-1}). T_{WP} was considered to be homogeneous for each well plate due to the high thermal conductivity of the aluminium compared to that of the surrounding gas (more than 9000 times greater) (Perry and Green, 2008). Similarly to the estimation of the vial bottom temperature (T_b) during tests with vials, T_{WP} was theoretically calculated for each well plate during tests without vials as follows:

$$T_{WP} = T_{sat} + \frac{\dot{Q}_{WP} l_{ice}}{\lambda_{ice} A_{WP}} \quad (5)$$

The calculated T_{WP} were in agreement (< 0.9 °C difference) with the values recorded by the Tempris probes inside the well plates.

The heat transfer coefficient between the well plate and the high-throughput vial bottom K_{HV} can be expressed according to the following equation:

$$K_{HV} = \frac{\dot{Q}_{HV}}{A_{HV}\left(T_{WP} - T_b\right)} = \frac{\dot{m}_{HV}\Delta H_{sub}}{A_{HV}\left(T_{WP} - T_b\right)} \quad (6)$$

Since T_{WP} was not monitored during the experiments with vials, we applied the following approach to determine the heat transfer coefficient K_{HV}: if we assume that the heat flows received individually by the 96 high-throughput vials in the well plate came only from the well plate, the heat flow received by the well plate and the vials are directly related:

$$\dot{Q}_{WP} = \sum_{i=1}^{96} \dot{Q}_{HV} \quad (7)$$

The value of T_{WP} was estimated using equations (4) and (7) as:

$$T_{WP} = T_{shelf} - \frac{\sum_{i=1}^{96} \dot{Q}_{HV}}{A_{WP} K_{WP}} \quad (8)$$

The 1000-µL vials protruded from the well plate and were more exposed to heat flow contributions from the freeze dryer. The assumption that the heat flows received by the vials came only from the well plate was presumably more realistic for the 500-µL vials than for the 1000-µL vials; therefore, T_{WP} values during tests with 1000-µL vials were considered to be the same as during the test with the 500-µL vials in the same well plate type.

K_V, K_{WP}, and K_{HV} can be related in a simple way under the hypothesis that all high-throughput vials and all the wells in a well plate had the same geometry and that all vials had the same heat transfer coefficients. In this way, heat flows can be expressed using the following equations:

$$96\dot{Q}_{HV} = \dot{Q}_{WP} \tag{9}$$

$$96\dot{Q}_{HV} = 96A_{HV}K_{HV}(T_{WP} - T_b) \tag{10}$$

$$\dot{Q}_{WP} = A_{WP}K_{WP}\left(T_{shelf} - T_{WP}\right) \tag{11}$$

$$96\dot{Q}_{HV} = 96A_{HV}K_V\left(T_{shelf} - T_b\right) \tag{12}$$

From equations (9) to (11), we obtain:

$$\dot{Q}_{HV}\left(\frac{1}{A_{HV}K_{HV}} + \frac{96}{A_{WP}K_{WP}}\right) = T_{shelf} - T_b \tag{13}$$

Equations (12) and (13) give:

$$\dot{Q}_{HV}\left(\frac{1}{A_{HV}K_V}\right) = T_{shelf} - T_b \tag{14}$$

Finally, the apparent heat transfer coefficient between the shelf and the high-throughput vial bottom can be expressed as:

$$\frac{1}{K_V} = \frac{1}{K_{HV}} + \frac{96A_{HV}}{A_{WP}K_{WP}} \tag{15}$$

Theoretical description of the heat transfer coefficients K_{WP} and K_{HV}

The heat transfer coefficients K_{WP} between the shelf and the well plate and K_{HV} between the well plate and the high-throughput vial can be described as the sum of the contribution of three heat transfer mechanisms:

$$K_{WP} = K_{WP}^{cc} + K_{WP}^{rad} + K_{WP}^{gc} \tag{16}$$

$$K_{HV} = K_{HV}^{cc} + K_{HV}^{rad} + K_{HV}^{gc} \tag{17}$$

where K_{WP}^{cc} and K_{HV}^{cc} represent the thermal conctact conduction between the shelf and the well plate, and between the well plate and the vial, respectively; similarly, K_{WP}^{rad} and K_{HV}^{rad} represent the thermal radiation;

and K_{WP}^{gc} and K_{HV}^{gc} account for the thermal conduction through the gas entrapped in the bottom curvature of the well plate and the vial, respectively.

Heat transfer coefficient by thermal contact conduction K_{WP}^{cc} and K_{HV}^{cc}

Most authors (Pikal et al., 1984; Pisano et al., 2011; Scutellà et al., 2017a; von Graberg, 2011) considered contact conduction as a constant value independent of the operating conditions. Therefore, K_{WP}^{cc} and K_{HV}^{cc}, were considered as temperature- and pressure-independent. Scutellà et al. (2017a) assumed that the contact conduction between the shelf and serum vials was proportional to the vial-shelf contact area. Analogously, the contact conduction coefficient between the well plate and the high-throughput vials K_{HV}^{cc} was considered to be proportional to the contact area between the vial bottom and the well plate (A_{HV}^{C}):

$$K_{HV}^{cc} = k_{HV}^{cc} A_{HV}^{C} \tag{18}$$

where k_{HV}^{cc} (W.m^{-4}.K^{-1}) is an empirical constant of proportionality.

Heat transfer coefficient by thermal radiation K_{WP}^{rad} and K_{HV}^{rad}

K_{WP}^{rad} *and* K_{HV}^{rad} were calculated according to the Stefan-Boltzmann formula for grey diffuse surfaces:

$$K_{WP}^{rad} = \sigma F_{WP}\left(T_{shelf} + T_{WP}\right)\left(T_{shelf}^{2} + T_{WP}^{2}\right) \tag{19}$$

$$K_{HV}^{rad} = \sigma F_{HV}(T_{WP} + T_{b})(T_{WP}^{2} + T_{b}^{2}) \tag{20}$$

where σ is the Stephan-Boltzmann constant (W.m^{-2}.K^{-4}), and the view factors F_{WP} and F_{HV} were calculated as for two parallel surfaces (Perry and Green, 2008):

$$F_{WP} = \frac{1}{\frac{1-\varepsilon_{shelf}}{\varepsilon_{shelf}} + \frac{1-\varepsilon_{WP}}{\varepsilon_{WP}} + 1} \tag{21}$$

$$F_{HV} = \frac{1}{\frac{1-\varepsilon_{WP}}{\varepsilon_{WP}} + \frac{1-\varepsilon_{HV}}{\varepsilon_{HV}} + 1} \tag{22}$$

where ε_{shelf}, ε_{WP}, and ε_{HV} are the emissivity values of the shelf, the well plate and the high-throughput vial, respectively.

Heat transfer coefficient by thermal conduction through the gas K_{WP}^{gc} and K_{HV}^{gc}

Three gas conduction regimes occur within the usual chamber pressure range during sublimation (< 15 Pa): free molecular, transition and continuous regimes. Pikal (2000) modelled the heat transfer

coefficient for conduction through the gas trapped between two parallel surfaces assuming the transition regime as:

$$K_{WP}^{gc} = \frac{\alpha_{WP} \Lambda_o P_C}{1 + \frac{l_{WP}}{\lambda_{gas}^{cont}} \alpha_{WP} \Lambda_o P_C} \quad (23)$$

$$K_{HV}^{gc} = \frac{\alpha_{HV} \Lambda_o P_C}{1 + \frac{l_{HV}}{\lambda_{gas}^{cont}} \alpha_{HV} \Lambda_o P_C} \quad (24)$$

where α_{WP} and α_{HV} are the thermal accommodation coefficients related to the quality of momentum exchange between the gas molecules and the solid surfaces (shelf and well plate, and well plate and vial, respectively), Λ_0 (W.m^{-2}.K^{-1}.Pa^{-1}) is the heat transfer coefficient of the gas at 0 °C in a free molecular regime, P_C (Pa) is the chamber pressure, l_{WP} and l_{HV} are the average distances between the solid surfaces, and λ_{gas}^{cont} (W.m^{-1}.K^{-1}) is the thermal conductivity of the water vapour in a continuous regime. l_{HV} was considered to be the average between the maximum and minimum vial bottom concavity.

Theoretical description of the heat transfer coefficient K_V

The heat transfer coefficient between the shelf and the high-throughput vial bottom K_V corresponds to an apparent heat transfer coefficient. Consequently, its representation as the sum of the three heat transfer contributions described above has no real physical meaning due to the presence of the well plate. However, for sake of comparison with the large existing body of literature, the following equation was used to represent the evolution of the coefficient K_V with the chamber pressure by analogy with serum vials (Pikal et al., 1984; Pikal, 2000; Pisano et al., 2011; Scutellà et al., 2017a; von Graberg, 2011):

$$K_V = K_V^{cc} + K_V^{rad} + \frac{\alpha_V \Lambda_o P_c}{1 + \frac{l_V}{\lambda_{gas}^{cont}} \alpha_V \Lambda_o P_c} \quad (25)$$

where, K_V^{cc} and K_V^{rad} were considered to be constants.

Calculation of K_V distributions based on high-throughput vial geometry

The impact of the vial bottom-well plate contact area A_{HV}^{C} on the global heat transfer coefficient K_V was evaluated for both well plate types (A-type and B-type) and both vial sizes (500-µL and 1000-µL vials) at chamber pressures of 4, 6, 12, 25, and 65 Pa. A chi-square goodness-of-fit test was performed with the A_{HV}^{C} values from the imprint tests, indicating that the data came from a normal distribution at a 0.05

significance level. K_V distributions based on vial geometry were obtained using the mean value and standard deviation of A_{HV}^C and equations (15), (16), and (17).

Calculation of K_V distributions in serum vials

K_V distributions in high-throughput vials were compared to K_V distributions in serum vials calculated based on the work of Scutellà et al. (2017a) – considering serum vials placed in the centre of the shelf. K_V distributions in serum vials were obtained using equation (25) and injecting two normal distributions: (*i)* one normal distribution of the distance between the shelf and the serum vial (l_V^{ser}); and (*ii)* one normal distribution of the serum vial-shelf contact area (A_{ser}^C) in:

$$K_{V,ser}^{cc} = A_{ser}^C k_{ser}^{cc} \tag{26}$$

where k_{ser}^{cc} is an empirical constant for contact conduction between the shelf and serum vials. Normal distributions were created based on the mean value and standard deviations of l_V^{ser} and A_C^{ser} in Table 1.

Simulation of the product temperature distribution using K_V distributions

Product temperature distributions were calculated using the approach proposed by Scutellà et al. (2017a) based on K_V distribution. For high-throughput vials, K_V values were the experimental distribution of the *96-Well Freeze-Drying Systems*. For serum vials, K_V values were the distribution obtained as described in *Calculation of K_V distributions in serum vials*. Product temperatures were calculated for a 5% sucrose solution considering a shelf temperature of -15 °C and five chamber pressures (4, 6, 12, 25, and 65 Pa). The mass flow ($\dot{m}$) during sublimation was related to the pressure difference between the chamber (P_C) and the ice sublimation front (P_{sat}) as (Pikal et al., 1984):

$$\dot{m} = \frac{A_{in}(P_{sat} - P_C)}{R_P} \tag{27}$$

where R_P (Pa.s.m^2.kg^{-1}) is the area-normalized product resistance, and A_{in} (m^2) is the inner bottom area of the vial. The R_P value was taken from literature (Konstantinidis et al., 2011) for a dried layer of 5% sucrose with a thickness of 0.5 cm, as reported in Table 1. To simulate the product temperature distribution, the non-linear system composed of equations (1) to (3) and (27) was solved for each K_V value, considering the temperature at the bottom of the vial (T_b) as the product temperature (T_p).

Results and discussion

Effect of the well plate type and vial size on the apparent heat transfer coefficient between the shelf and the high-throughput vial bottom K_V

The values of the apparent heat transfer coefficient K_V were calculated for 576 500-µL vials and 573 1000-µL vials at a shelf temperature of -15 °C for five chamber pressures (from 4 to 65 Pa). High-throughput vials located at the edge of the well plates (white circles in Figure *2*) presented greater K_V values than those located in the centre (green circles in Figure *2*); increasing up to 10% for 500-µL vials and 25% for 1000-µL vials at a chamber pressure of 4 Pa; consequently, they were not considered in this study.

Figure 3a and Figure *3*b display the evolution of the average K_V value with the chamber pressure for the 500-µL and 1000-µL vials, respectively. The data concerning the two well plate types (A-type presenting a brilliant surface finish, and B-type presenting a matte surface finish) are reported on each figure, as well as the K_V evolution with the chamber pressure for serum vials in the centre of the shelf obtained by Scutellà et al. (2017a). The experimental data obtained using high-throughput vials and serum vials (Scutellà et al., 2017a) were acquired using the same freeze dryer (Epsilon 2-25D, Martin Christ).

Regardless of the well plate type and vial sizes (500-µL and 1000-µL), K_V of high-throughput vials were more than twice as great as K_V of serum vials at chamber pressures lower than 25 Pa. Therefore, the heat transfer per vial cross-section was more efficient in high-throughput vials placed in well plates than in serum vials placed directly on the shelf. Von Graberg (2011) measured K_V of 500-µL vials using the *96 Well Freeze-Drying System* manufactured by VirTis, and the values are included in Figure 3a. Results obtained by Von Graberg (2011) are within the range of our K_V values considering both well plate types. Coefficients of equation (25) were estimated using experimental data, and their values are presented in Table *2*.

The average K_V values were greater for B-type well plates (orange symbol in Figure 3) than for A-type (blue symbol in Figure 3). At a chamber pressure of 4 Pa, the K_V difference between well plate types appeared to be quite narrow (lower than 12%), and then increased with increasing chamber pressure to reach 34% for 500-µL vials and 24% for 1000-µL vials at 65 Pa.

Furthermore, when considering chamber pressures lower than 25 Pa, K_V values of 1000-µL vials were an average of 21% greater than K_V values of 500-µL vials. Since the two vial sizes differed only by vial height, this reported K_V difference could be ascribed to an extra heat contribution received by the top

portion of 1000-µL vials protruding from the well plate. This possible extra heat contribution is reflected in the unphysical α_V values for 1000-µL vials (Table 2); these estimated values were greater than the highest theoretical accommodation coefficient between two surfaces (≈ 1; Pikal, 2000), whereas 500-µL vials presented α_V values below 0.9.

Since there was no direct contact between the shelf and high-throughput vials, the coefficients of equation (25) reported in Table 2 do not have a physical meaning. To better understand the role of the well plate and the vial on the heat transfer mechanisms, we broke down the apparent heat transfer coefficient K_V in two heat transfer phenomena in series: (*i)* from the shelf to the well plate; and (*ii)* from the well plate to the vial.

Effect of chamber pressure on the heat transfer coefficients between the shelf and the well plate (K_{WP}) and between the well plate and the vial (K_{HV})

K_{WP} values were calculated using the data of the sublimation experiments carried out without vials inside the well plates and equations (3) to (5), while K_{HV} were calculated using the data of the sublimation experiments with vials and equations (2), (3), (6) and (8). Only the K_{HV} of vials located in the centre of the well plates (represented as green circles in Figure *2*) were considered. Figure 4a shows the evolution of K_{WP} values with the chamber pressure for both well plate types (A-type and B-type), and Figure 4b presents the evolution of K_{HV} for both well plate types and vial sizes (500-µL and 1000-µL). K_{WP} values varied with chamber pressure, increasing five times from 4 to 65 Pa, whereas K_{HV} values appeared to be quite constant with the chamber pressure.

Table 3 presents the values of the coefficients presented in equations (16), (17), (23), and (24) fitted with the K_{WP} and K_{HV} data. The absence of significant pressure dependence of K_{HV} resulted in numerical difficulties to estimate the parameter α_{HV}, therefore causing the significant variation of this parameter for each combination of well plate type and vial size.

The contributions of the heat transfer mechanisms to the heat transfer coefficients K_{WP} and K_{HV} were calculated using equations (16), (17), and (19) to (24), and the fitted coefficients are reported in

Table 3. Figure 5 shows the relative contribution of contact conduction (K_{WP}^{cc} and K_{HV}^{cc}), conduction through the gas (K_{WP}^{gc} and K_{HV}^{gc}), and radiation (K_{WP}^{rad} and K_{HV}^{rad}) to K_{WP} (Figure 5a) and K_{HV} (Figure 5b). Gas conduction (K_{WP}^{gc}) was the greatest contributor to K_{WP}, increasing from 62% at 4 Pa to 93% at 65 Pa (average between well plate types); contact conduction (K_{HV}^{cc}) was the greatest contributor to K_{HV}, representing 96% at 4 Pa and 73% at 65 Pa (average between well plate types and vial sizes).

The contribution to heat transfer by radiation was very low (< 7%), regardless of the heat transfer coefficient (K_{WP} and K_{HV}) and the chamber pressure, whereas the radiation contribution represents around 20 to 30% of K_V for serum vials at chamber pressures below 10 Pa (Scutellà et al., 2017a).

Several authors reported the importance of the vial bottom curvature on heat transfer between the shelf and the bottom of the serum vials (Brülls and Rasmuson, 2002; Pisano et al., 2011; Scutellà et al., 2017a). When considering high throughput vials, the vial bottom curvature is small enough to consider the divisor in equation (24) equal to 1 ($l_{HV} \ll \frac{\lambda_{gas}^{cont}}{\alpha_{HV} \Lambda_o P_C}$), so l_{HV} did not have an impact on K_{HV}. This explains the quasi linear pressure dependence of K_{HV} (Figure 4b). The only gas layer thickness involved in the gas conduction that impacted K_V was the apparent distance between the bottom shelf and the well plate bottom (l_{WP}) through its effect on K_{WP}.

Regarding the effect of the well plate type on K_{WP}, A-type well plates exhibited lower K_{WP} values than B-type well plates, in particular for chamber pressure higher than 25 Pa. The effect of the well plate type on K_{WP} could be ascribed to the circular marks on the bottom surface of A-type well plates (Figure 1b); these marks could reduce the number of contact points with the shelf, which explains the lower K_{WP}^{cc} value observed in Table 3 compared to that of B-type well plates. Furthermore, these surface deformations (observed as marks) could leave more space for trapped gas between the shelf and the well plate, which is in agreement with the higher l_{WP} values for A-type well plates than for B-type well plates.

In Figure 4b, we observe that 1000-µL vials exhibited higher K_{HV} values than 500-µL (by approximately 50%), which was not initially expected since both vial sizes have similar bottom geometry and differ only in height. As was previously observed for K_V data, 1000-µL vials may have received extra heat via the portion of vials that protruded from the well plate. Furthermore, K_{HV} values of 500-µL vials in B-type well plates were more than 44% greater than those in A-type well plates, which could be ascribed to a higher contribution of heat transfer by contact conduction (K_{HV}^{cc}) and, therefore, to a better contact between the bottom of the wells and the vials. The internal surface of the well bottoms in A-type well plates also

presented noticeable manufacturing marks. Therefore, the number of contact points between the wells and the vials might have varied among well plate types, impacting K_{HV}^{cc}.

Equation (15) made it possible to calculate the heat transfer resistance induced by the well plate $\{[K_{WP}A_{WP} / (nA_{HV})]^{-1}\}$ and by the vial $[(K_{HV})^{-1}]$. The dominant resistance to the heat transfer was between the shelf and the well plate, representing more than 70% of the total heat transfer resistance for chamber pressures lower than 12 Pa. This explains the clear pressure dependence of K_V (Figure 3), following a trend similar to that of K_{WP} (Figure 4a).

The values of the heat transfer resistances $[K_{WP}A_{WP} / (nA_{HV})]^{-1}$ and $(K_{HV})^{-1}$ were considerably lower than $(K_V)^{-1}$ for serum vials determined by Scutellà et al. (2017a), 3 times and 20 times lower, respectively (at chamber pressures lower than 12 Pa). The low values of $[K_{WP}A_{WP} / (nA_{HV})]^{-1}$ were due to the high quality of momentum exchange between the gas molecules and the well plate surface; as previously mentioned, the thermal accommodation coefficients between the shelf and the well plate (> 0.8, Table 3) were greater than that between the shelf and serum vials (≈ 0.33; Scutellà et al., 2017a). Furthermore, the low values of $(K_{HV})^{-1}$ were due to the flatness of the high-throughput vial bottoms, which increased the contact area (A^C, Table 1) and the heat transfer by contact conduction; A_{HV}^C represents 32% of the outer bottom area of high-throughput vials, while A_{ser}^C is only 8% of the outer bottom area of serum vials. Finally, the low $[K_{WP}A_{WP} / (nA_{HV})]^{-1}$ and $(K_{HV})^{-1}$ explain why the high-throughput system was more effective to transfer the heat from the shelf to the vials than placing serum vials on the shelf.

Impact of vial geometry on the K_V distribution and predicted product temperature distribution

Figure 6 shows the distributions of the experimental K_V values of high-throughput vials in positions represented as green circles in Figure 2 (vials in the centre of the well plate), as well as the K_V distributions of serum vials placed in the centre of the shelf calculated from the results obtained by Scutellà et al. (2017a). Regardless of the well plate type (A-type or B-type) and vial size (500-µL or 1000-µL), we observed a significant variability in the K_V values, and the standard deviation (SD) increased with pressure from approximately 4 to 10 $W.m^{-2}.K^{-1}$. The K_V distribution of high-throughput vials appeared considerably wider than that of serum vials, with a coefficient of variation for high-throughput vials of approximately 14%, compared to 4-8% for serum vials (Scutellà et al., 2017a). The

measurement uncertainty of K_V was estimated to be approximately 1%, and could therefore not explain the K_V variability observed.

By following the approach proposed by Scutellà et al. (2017a), we investigated the impact of vial geometry, in particular the contact area between the vial and the well plate on K_V variability. As mentioned before, l_{HV} values were too low to have an impact on K_{HV} ($l_{HV} \ll \frac{\lambda_{gas}^{cont}}{\alpha_{HV} \Lambda_o P_C}$), so its impact on K_V was not considered in this study. K_{HV}^{cc} can be expressed as a function of an empirical constant k_{HV}^{cc} and the vial bottom-well plate contact area A_{HV}^{C} [equation (18)]. A normal distribution of A_{HV}^{C} values was created based on the mean value and standard deviation estimated by the imprint test. The simulated K_V distributions obtained using the A_{HV}^{C} normal distribution and equations (15), (17) and (18) are plotted as red lines in Figure 6. These simulated distributions were similar to the experimental distributions. As a result, A_{HV}^{C} variability could potentially explain the heterogeneities of the heat flows received by vials in the centre of the same well plate. Similarly, Scutellà et al. (2017a) revealed the importance of the contact area on the variability of K_V of serum vials at chamber pressures lower than 15 Pa.

Product temperature (T_p) is a key process parameter governing product quality, in particular the visual aspect of the freeze-dried cake. Vial-to-vial variability of the heat and mass transfer during primary drying could result in T_p heterogeneities within the vial batch and, thus, in potential product quality variations. Figure 7 shows the T_p distributions based on the experimental K_V distributions of high-throughput vials and artificial K_V distributions of serum vials at different chamber pressures, considering a constant product resistance (1.248×10^5 Pa.s.m^2.kg^{-1}, Table 1) and a shelf temperature of -15 °C. Greater K_V values are associated with higher T_p values. As expected from K_V results, T_p increased with chamber pressure for all vial geometries, and T_p were greater for high-throughput vials than for serum vials. However, the temperature gap between both vial geometries decreased with chamber pressure from 8.3 °C at 4 Pa to 2.1 °C at 65 Pa. The variability of T_p using high-throughput vials was estimated to be approximately 2.6 °C at 12 Pa and 3.3 °C at 4 Pa, considering +/- 3 times the standard deviation reported in Figure 7 that includes 99.7% of the vials. Therefore, a temperature safety margin of 3 °C is recommended when designing freeze-drying cycles using high-throughput vials placed in the centre of a well plate, regardless of the well plate type and vial size. This margin is in agreement with the recommendations of Nail and Searles (2008) when using a design space. However, it is greater than

the 2 °C proposed by Scutellà et al. (2017a) for serum vials because of the greater K_V standard deviations of high-throughput vials.

T_p values for each well plate type and vial size (500-µL and 1000-µL) differed due to the differences observed in K_V. When considering chamber pressures below 12 Pa, T_p values using 1000-µL vials were 1.6 °C higher than those using 500-µL (average increase considering both well plate types), and T_p values using B-type well plates were 1.1 °C higher than values using A-type well plates (average increase considering both high-throughput vial sizes). Therefore, the vial size and well plate type should be taken into account during freeze-drying experiments using high-throughput vial systems.

Process scale-up from high-throughput to serum vials and vice versa

High-throughput vial systems are increasingly used to accelerate the formulation development stage since they require less active ingredients, and more formulations could be tested per freeze-drying cycle. Once a pool of formulations is pre-selected based on their aptitude to preserve the active ingredient, the final formulation is usually selected based on the physical properties: the collapse temperature and the glass transition temperature of the maximally freeze-concentrated phase (Pikal and Shah, 1990). After selecting a given formulation using high-throughput vials, it is necessary to define the operating conditions during freeze-drying in the container used at industrial scales – in serum vials, for example. Conversely, it could be necessary to "translate" operating conditions of cycles developed using serum vials to cycles using high-throughput vials. The criterion for the "translation" between containers will be to maintain the same product thermal history during the process, in particular the same product temperature during sublimation. The strategies we propose to operate process scale-up from high-throughput to serum vials and scale-down from serum to high-throughput vials are analogous and consist of two steps: (*i)* creating a "design space" (Nail and Searles, 2008) to identify the optimal operating conditions using the departure vial geometry; and (*ii)* constructing a graphical solution to define the design space of the final vial geometry considering the operating condition selected for the departure vial geometry.

Figure 8a shows the design space for freeze-drying a 5% sucrose solution using high-throughput 500-µL vials in an A-type well plate; analogous figures are obtained applying the same approach to other high-throughput vial sizes and well plate types. Design spaces link the operating conditions during primary drying (i.e., shelf temperature and chamber pressure) with the predicted sublimation mass flows ($\dot{m}$) and the product temperature (T_p), serving as a graphical solution of equations (1) to (3), (25), and

(27). The grey area in Figure 8a represents the operating conditions that involve a T_p lower than the maximum allowed product temperature. In this case, it was considered the collapse temperature of a 5% sucrose solution (-32 °C; Greco et al., 2013) minus the temperature safety margin defined in the previous section of this study (3 °C) for high-throughput vials in the centre of the well plate. This grey area represents the "safe" combinations of operating conditions that ensure a high quality freeze-dried product. It is possible to optimize the freeze-drying process by selecting an operating condition leading to the highest sublimation rate. For example, in Figure 8a, we have chosen the black square frame as the combination of operating conditions (a shelf temperature of -25 °C and a chamber pressure of 5 Pa) that allow the maximisation of the sublimation rate in high-throughput vials (y-axis), at a T_p of -36 °C.

Figure 8b presents the graphical method we built to identify the operating conditions using serum vials at the same product temperature reached during previous tests using high-throughput vials (scale-up). The graph links the shelf temperature (T_{shelf}^{ser}) and chamber pressure (P_C^{ser}) using serum vials to iso-T_p curves represented as linear colour maps obtained by solving equations (1) to (3), (25) and (27) applied to serum vials. This system of equations used to model the heat and mass transfer for each vial geometry has two degrees of freedom; hence, we only need to fix two inputs to define the system. Interesting inputs to fix from a practical point of view could be: the chamber pressure, the shelf temperature, T_p, or $\dot{m}$. Figure 8b was designed for the chamber pressure value previously selected by process optimisation in high-throughput vials using Figure 8a (P_C^{HT} = 5 Pa); consequently, iso-T_p curves are associated with only one shelf temperature condition when considering high-throughput vials (T_{shelf}^{HT}). For our example, all the different combinations of T_{shelf}^{ser} and P_C^{ser} represented in the iso-T_p= -36 °C (T_{shelf}^{HT} = -25 °C) correspond to the operating conditions using high-throughput vials represented as a black square frame in Figure 8a. It is then possible to select the optimal combination of operating conditions to maximise the sublimation rate using serum vials (colour scale in Figure 8b) by moving towards lower P_C^{ser} values in the iso-T_p curve (yellow part of the iso-T_p= -36 °C curve). Nevertheless, working at low chamber pressures could involve a greater edge effect between serum vials (Pisano et al., 2011; Scutellà et al., 2017b) and/or require a finer control of the chamber pressure to avoid process deviations. We selected a chamber pressure (P_C^{ser}) of 10 Pa (moderate value), corresponding to a shelf temperature (T_{shelf}^{ser}) of -18 °C represented as the black square frame in Figure 8b, obtaining a mass flow rate in serum vials of 1.4×10^{-8} kg.s^{-1}. The grey area in Figure 8b represents the operating conditions that are safe to apply using serum vials and "translatable" between geometries. The limits of the grey area are:

the maximal T_p accepted at the top edge, the minimal pressure using serum vials at the left edge, the zero mass flow conditions using serum vials at the right edge (T_{sat} at P_C^{ser}), and the zero mass flow condition using high-throughput vials at the bottom edge (T_{sat} at P_C^{HT}).

Figure 8c and 8d illustrate the procedure applied when “translating” operating conditions from serum to high-throughput vials (scale-down). When using serum vials, the operating conditions represented by the black square frame in Figure 8c were selected: shelf temperature of -20 °C and chamber pressure of 10 Pa. Analogously to Figure 8b, the grey area in Figure 8d represents the safe area of operating conditions that could be applied with high-throughput and serum vials.

Conclusions

There is a growing demand from some pharmaceutical companies to consider the steps of formulation screening, process optimization, and scale-up in an integrated way. For this reason, the primary packaging of the final product is increasingly often defined in advance before starting the formulation development. The use of a high-throughput vial system to screen formulations during freeze-drying could accelerate the development of new pharmaceutical products. Additionally, identifying the operating conditions that entail the same product temperature when using the final production container (serum vials for instance) would lead researchers to develop representative processes at pilot or industrial scale. This identification will require forecasting heat transfer parameters and heterogeneities in both geometries. We established that the surface finish of the well plate and the height of the vials influence the heat transfer. Variations between well plate types were due to the conduction within the gas trapped between the shelf and the well plate, as well as the contact conduction at pressures lower than 12 Pa. Variations in the heat flow received by high-throughput vials in the centre of a well plate could be explained by the contact conduction between the well plate and the vial. The variability in the heat flow resulted in the identification of a product temperature safety margin of 3 °C for choosing the operating conditions to be applied during primary drying using a design space approach.

The heat transfer coefficients between the shelf and the vial bottoms (K_V) were approximately three times greater in high-throughput vials than in serum vials at chamber pressures lower than 12 Pa; consequently, the predicted product temperatures were in average 8 °C higher using high-throughput vials than serum vials at a shelf temperature of -15 °C and chamber pressures lower than 12 Pa. A novel diagram representing the operating conditions at the same product temperature in high-throughput vials and serum vials is proposed. This diagram presents a range of operating conditions that are possible to scale-up or scale-down.

Further research should be conducted on the impact of the vial position in the well plate on the heat flow received.

References

Brülls, M., Rasmuson, A., 2002. Heat transfer in vial lyophilization. Internation journal of pharmaceutics 246, 1–16.

Fonseca, F., Cenard, S., Passot, S., 2015. Freeze-Drying of Lactic Acid Bacteria, in: Wolkers, W.F., Oldenhof, H. (Eds.), Cryopreservation and Freeze-Drying Protocols, Methods in Molecular Biology. Springer, New York, NY, pp. 477–488. https://doi.org/10.1007/978-1-4939-2193-5_24

Greco, K., Mujat, M., Galbally-Kinney, K.L., Hammer, D.X., Ferguson, R.D., Iftimia, N., Mulhall, P., Sharma, P., Kessler, W.J., Pikal, M.J., 2013. Accurate Prediction of Collapse Temperature using Optical Coherence Tomography-Based Freeze-Drying Microscopy. Journal of Pharmaceutical Sciences 102, 1773–1785. https://doi.org/10.1002/jps.23516

Haynes, W.M. (Ed.), 2014. CRC Handbook of Chemistry and Physics, 95th Edition, 95 edition. ed. CRC Press, Boca Raton; London; New York.

Konstantinidis, A.K., Kuu, W., Otten, L., Nail, S.L., Sever, R.R., 2011. Controlled nucleation in freeze-drying: Effects on pore size in the dried product layer, mass transfer resistance, and primary drying rate. Journal of Pharmaceutical Sciences 100, 3453–3470. https://doi.org/10.1002/jps.22561

Kuu, W.Y., Nail, S.L., 2009. Rapid freeze-drying cycle optimization using computer programs developed based on heat and mass transfer models and facilitated by tunable diode laser absorption spectroscopy (TDLAS). Journal of Pharmaceutical Sciences 98, 3469–3482. https://doi.org/10.1002/jps.21813

Murphy, D.M., Koop, T., 2005. Review of the vapour pressures of ice and supercooled water for atmospheric applications. Quarterly Journal of the Royal Meteorological Society 131, 1539–1565. https://doi.org/10.1256/qj.04.94

Nail, S., Searles, J., 2008. Elements of quality by design in development and scale-up of freeze parenterals. BioPharm International 21, 44–52.

Patel, S.M., Pikal, M.J., 2011. Emerging freeze-drying process development and scale-up issues. AAPS PharmSciTech 12, 372–378. https://doi.org/10.1208/s12249-011-9599-9

Perry, R.H., Green, D.O., 2008. Perry's chemical engineers' handbook, 8th ed. McGraw-Hill.

Pikal, M.J., 2000. Heat and mass transfer in low pressure gases: applications to freeze-drying, in: Transport Processes in Pharmaceutical Systems. Marcel Dekker, Inc., New York, pp. 611–686.

Pikal, M.J., 1994. Freeze-Drying of Proteins, in: Formulation and Delivery of Proteins and Peptides, ACS Symposium Series. American Chemical Society, pp. 120–133. https://doi.org/10.1021/bk-1994-0567.ch008

Pikal, M.J., Dellerman, K.M., Roy, M.L., Riggin, R.M., 1991. The Effects of Formulation Variables on the Stability of Freeze-Dried Human Growth Hormone. Pharm Res 8, 427–436. https://doi.org/10.1023/A:1015834724528

Pikal, M.J., Roy, M.L., Shah, S., 1984. Mass and Heat Transfer in Vial Freeze-Drying of Pharmaceuticals: Role of the Vial. Journal of Pharmaceutical Sciences 73, 1224–1237. https://doi.org/10.1002/jps.2600730910

Pikal, M.J., Shah, S., 1990. The collapse temperature in freeze drying: Dependence on measurement methodology and rate of water removal from the glassy phase. International Journal of Pharmaceutics 62, 165–186. https://doi.org/10.1016/0378-5173(90)90231-R

Pisano, R., Baressi, A.A., Fissore, D., 2011. Heat transfer in freeze-drying apparatus, in: Developments in Heat Transfer. Rijeka, Croatia, pp. 91–114.

Scutellà, B., Passot, S., Bourlés, E., Fonseca, F., Tréléa, I.C., 2017a. How Vial Geometry Variability Influences Heat Transfer and Product Temperature During Freeze-Drying. Journal of Pharmaceutical Sciences 106, 770–778. https://doi.org/10.1016/j.xphs.2016.11.007

Scutellà, B., Plana-Fattori, A., Passot, S., Bourlés, E., Fonseca, F., Flick, D., Tréléa, I.C., 2017b. 3D mathematical modelling to understand atypical heat transfer observed in vial freeze-drying. Applied thermal engineering 126, 226–236.

Trnka, H., Rantanen, J., Grohganz, H., 2015. Well-plate freeze-drying: a high throughput platform for screening of physical properties of freeze-dried formulations. Pharmaceutical development and technology 20, 65–73.

US Food and Drug Administration, 2009. Guidance for Industry: Q8(R2) pharmaceutical development. http://www.fda.gov/downloads/Drugs/.../Guidances/ucm073507.pdf (International Conference on Harmonization).

von Graberg, S., 2011. Freeze Drying from Small Containers: Heat and Mass Transfer and Implications on Process Design [WWW Document]. ResearchGate. URL https://www.researchgate.net/publication/296063173_Freeze_Drying_from_Small_Containers_Heat_and_Mass_Transfer_and_Implications_on_Process_Design (accessed 2.7.19).

Wagner, W., Saul, A., Pruss, A., 1994. International Equations for the Pressure Along the Melting and Along the Sublimation Curve of Ordinary Water Substance. Journal of Physical and Chemical Reference Data 23, 515–527. https://doi.org/10.1063/1.555947

Acknowledgments

The authors would like to thank Emanuele Tomba and Mohamed Belkacem (GSK) for reviewing this manuscript and Vincent Ronsse (technician) and Alain Philippart (operator) (GSK) for their help in data acquisition.

Conflicts of interest

Erwan Bourlés and Bernadette Scutellà are employees of the GSK group of companies. Juan Buceta participated in a post-graduate PhD programme at GSK. Stéphanie Passot, Fernanda Fonseca and Ioan Cristian Tréléa report no financial conflicts of interest.

Funding

This work was funded by GlaxoSmithKline Biologicals S.A., under a Cooperative Research and Development Agreement with the Institut National de la Recherche pour l'Agriculture, l'Alimentation et l'Environnement (INRAE) via the intermediary of the Unité Mixte de Recherche (UMR), Paris Saclay Food and Bioproducts Engineering (SayFood) at the INRAE, Versailles-Grignon Research Centre.

Author's contributions

Juan Buceta, Stéphanie Passot, Bernadette Scutellà, Erwan Bourlés, Fernanda Fonseca and Ioan Cristian Tréléa were involved in the conception and design of the study. Juan Buceta, Bernadette Scutellà and Erwan Bourlés acquired the data. Juan Buceta, Stéphanie Passot, Bernadette Scutellà, Erwan Bourlés, Fernanda Fonseca and Ioan Cristian Tréléa analysed and interpreted the results. All authors were involved in drafting the manuscript or critically revising it for relevant intellectual content. All authors had full access to the data and approved the manuscript before it was submitted by the corresponding author.

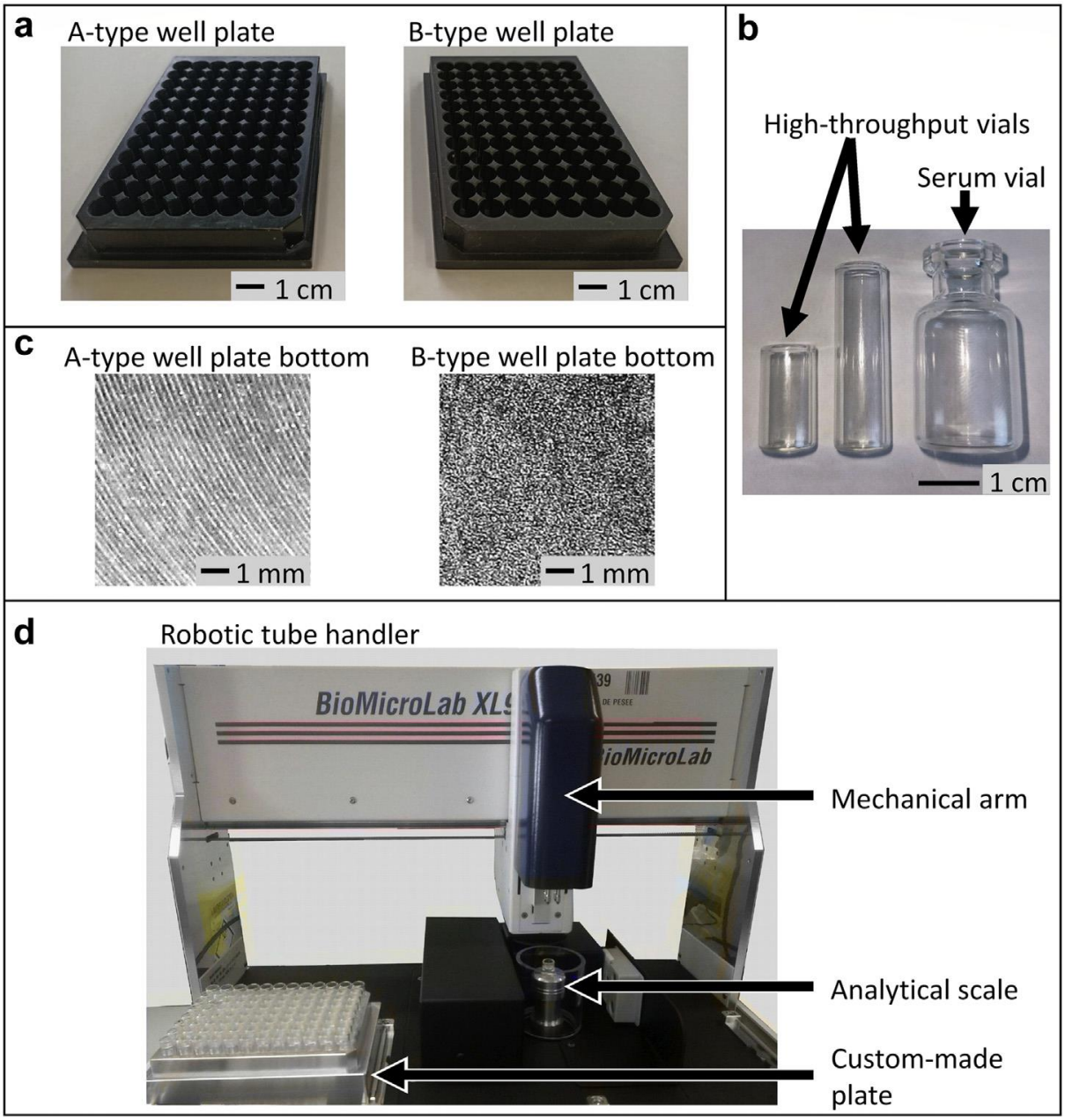

Figure 1 – *96-Well Freeze-Drying System* manufactured by VirTis composed of (a) well plates and (c) high-throughput glass vials; (b) close-ups of the well plate bottom surfaces; (d) the robotic tube handler specifically developed for weighing the high-throughput glass vials.

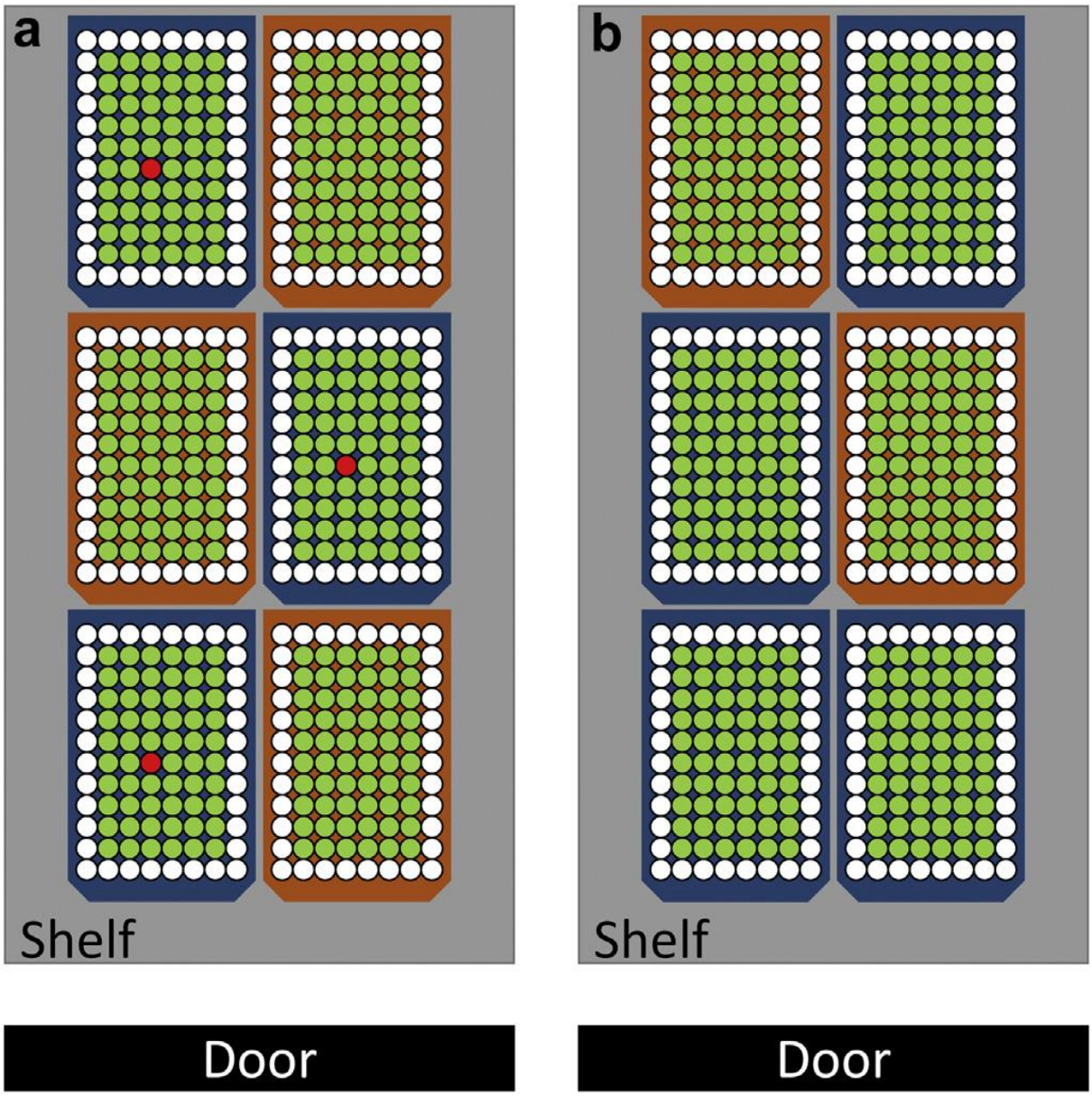

Figure 2 – Arrangement of the well plates on the freeze dryer shelf for tests with (a) 1000-µL vials, and (b) 500-µL vials; tests without vials were performed using the same well plate arrangement as (a). View of the shelf from the top not in scale. Well plate positions with A-type well plates are in blue, and B-type well plate positions are in orange. Circles represent vial positions, green circles represent positions considered for K_V and K_{HV} treatment, white circles represent positions on the edge of the well plate not considered in this work, and red circles represent vial positions with temperature probes during tests with 1000-µL vials.

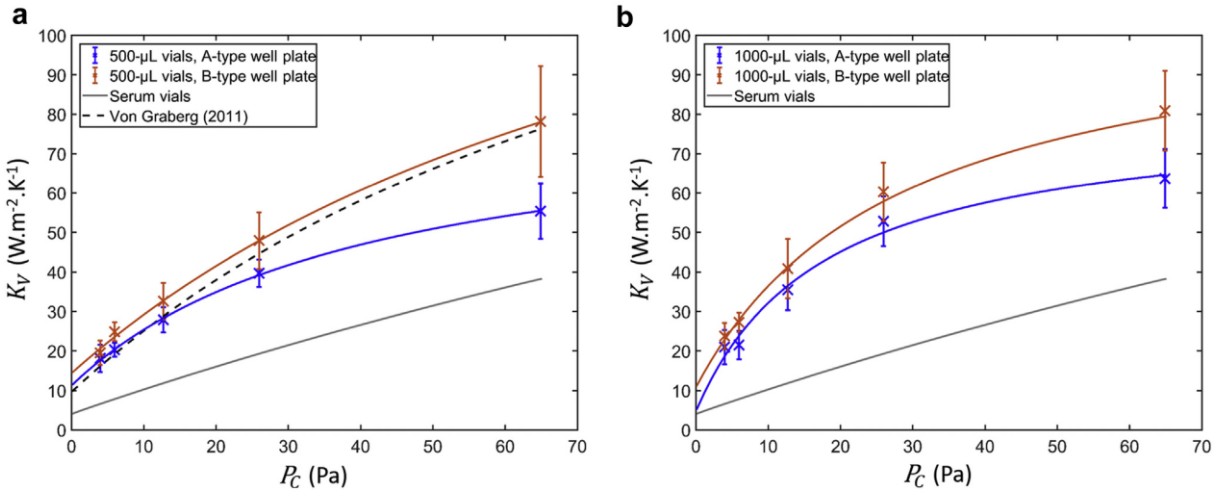

Figure 3 – Apparent heat transfer coefficients between the shelf and the vial bottom (K_V) vs. chamber pressure (P_C) for: (a) 500-µL vials, and (b) 1000-µL vials. The curves correspond to the values calculated with equation (25). Error bars represent standard deviations. K_V for serum vials are based on Scutellà et al. (2017a) represented in grey. K_V estimated by von Graberg (2011) are represented as a dotted black line; values were readjusted to have the same heat transfer area (A_{HV}) considered in our study.

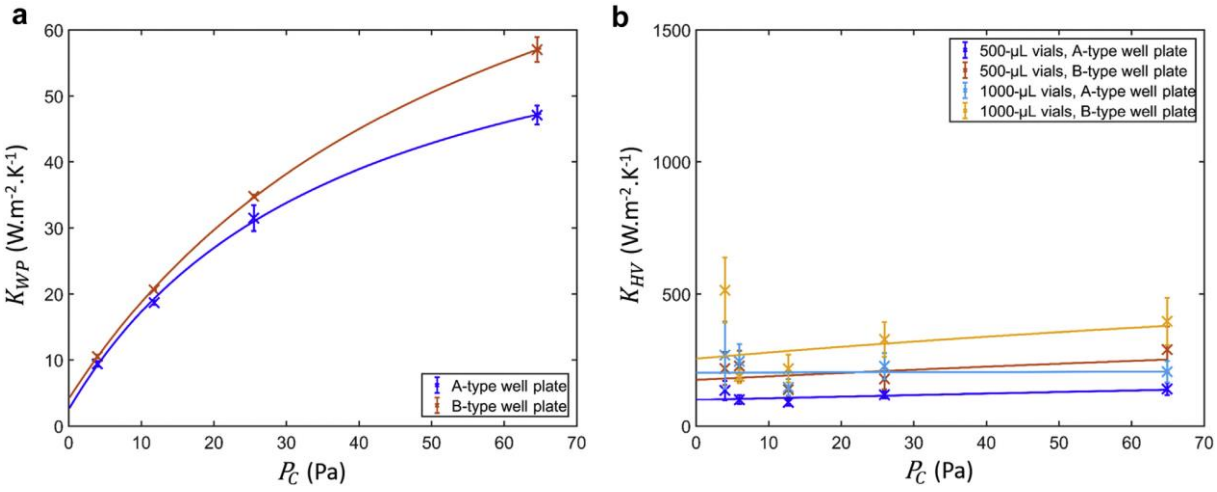

Figure 4 – Heat transfer coefficients (a) between the shelf and well plate bottom (K_{WP}), and (b) between the well plate and vial bottom (K_{HV}), vs. chamber pressure (P_C). The curves correspond to the values calculated with equations (16), (17) and (19) to (24). Error bars represent standard deviations.

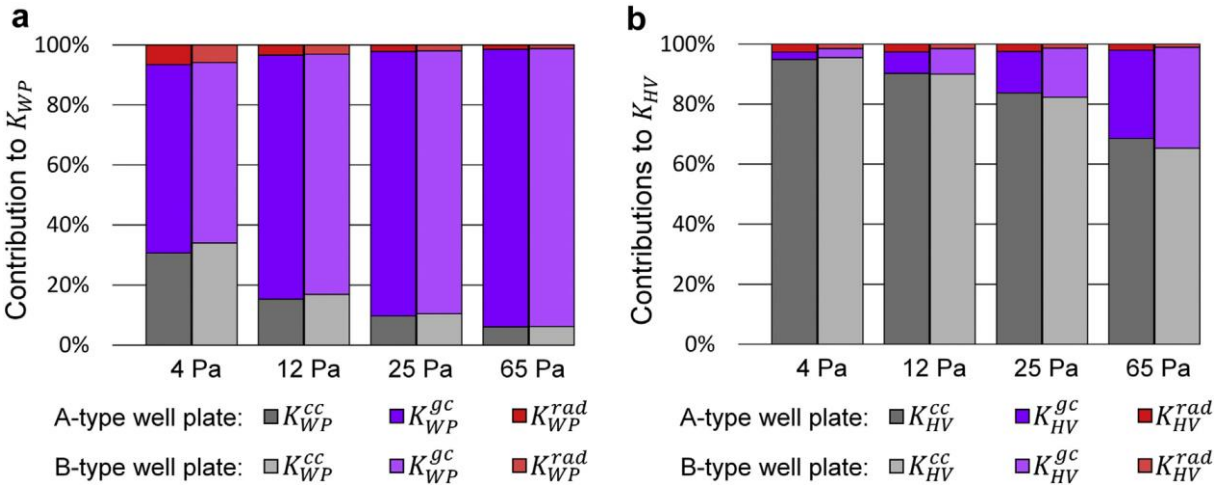

Figure 5 – Relative contributions of the heat transfer coefficients by contact conduction (K_{WP}^{cc}, K_{HV}^{cc}), conduction through the gas (K_{WP}^{gc}, K_{HV}^{gc}), and radiation (K_{WP}^{rad}, K_{HV}^{rad}) as percentages of the total heat transfer coefficients: (a) between shelf and wall plate (K_{WP}), and (b) between wall plate and vial (K_{HV}). K_{HV} values for 500-µL vials.

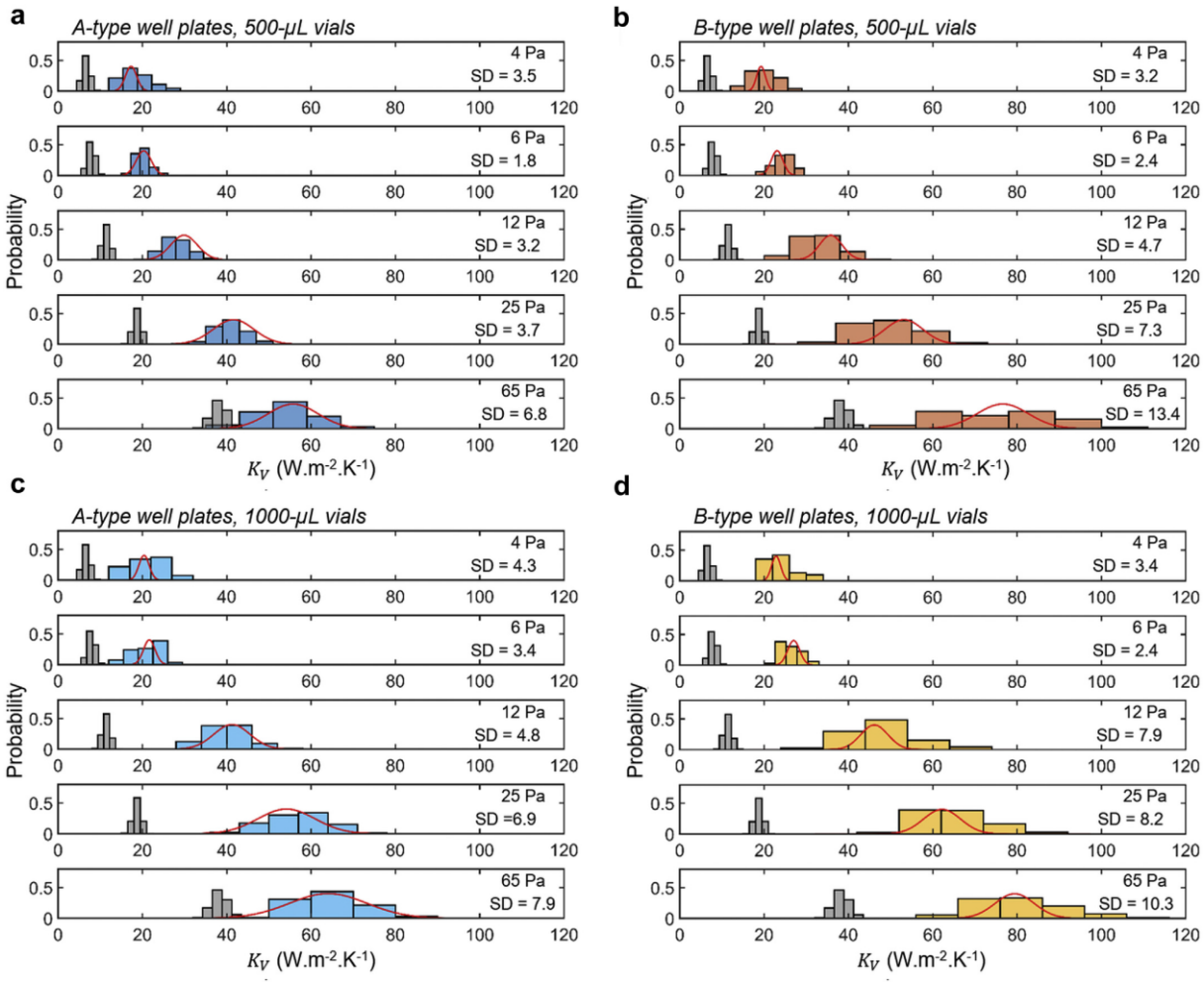

Figure 6 – Distributions of the heat transfer coefficient between the shelf and the vial (K_V) and their respective standard deviations (SD) for both well plate types and vial sizes. Distributions in grey are taken from Scutellà et al. (2017a) for serum vials. Red lines are the calculated K_V based on vial geometry variation (contact area) distributions. Results using: (a) 500-µL vials inside A-type well plates, (b) 500-µL vials inside B-type well plates, (c) 1000-µL vials inside A-type well plates, and (d) 1000-µL vials inside B-type well plates.

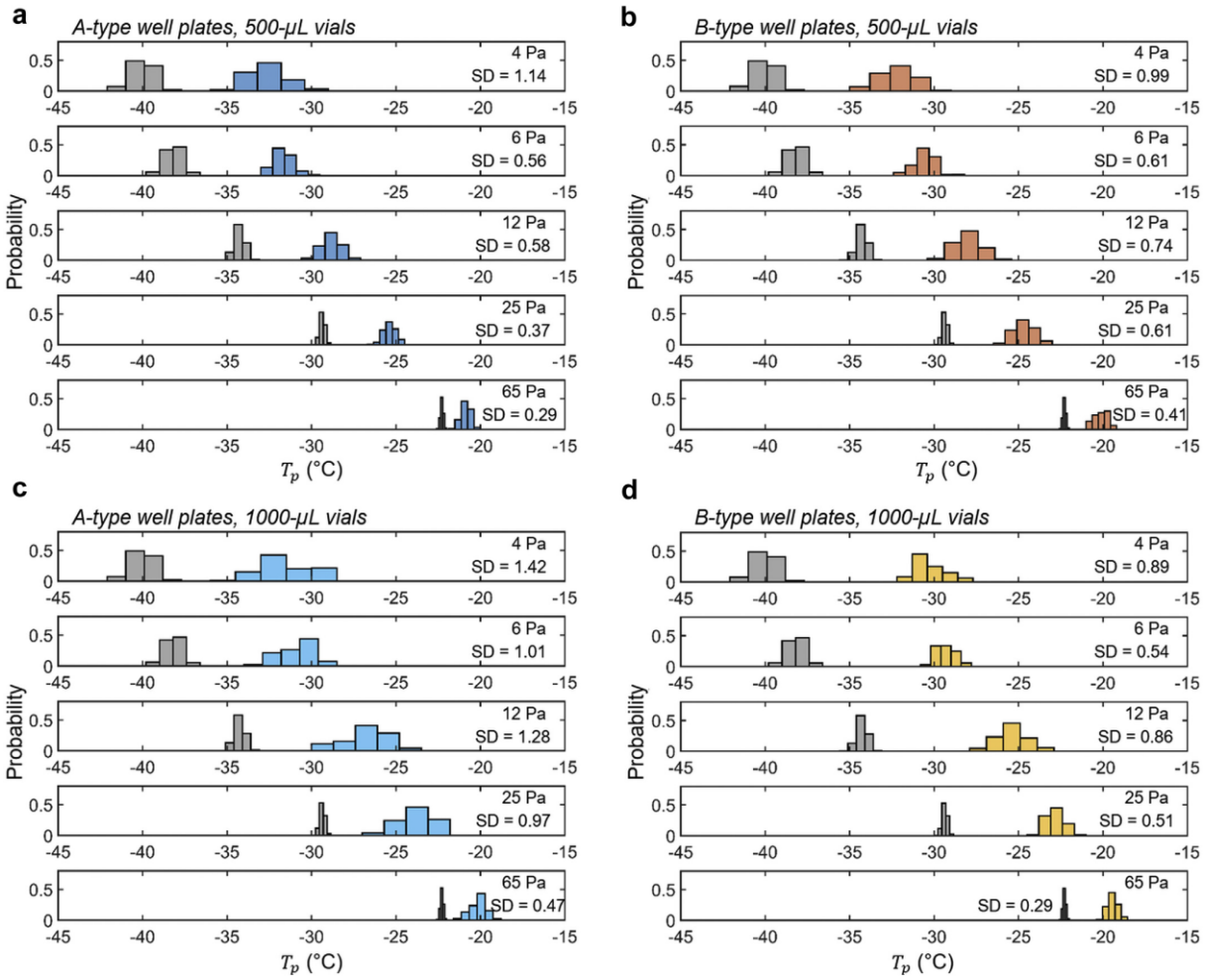

Figure 7 – Product temperature (T_P) distributions and standard deviations (SD) at shelf temperature (15 °C) obtained from the heat transfer coefficient between the shelf and the vial (K_V) for both well plate types and vial sizes. Distributions in grey are based on K_V taken from Scutellà et al. (2017a) for serum vials. Results using: (a) 500-µL vials inside A-type well plates, (b) 500-µL vials inside B-type well plates, (c) 1000-µL vials inside A-type well plates, and (d) 1000-µL vials inside B-type well plates.

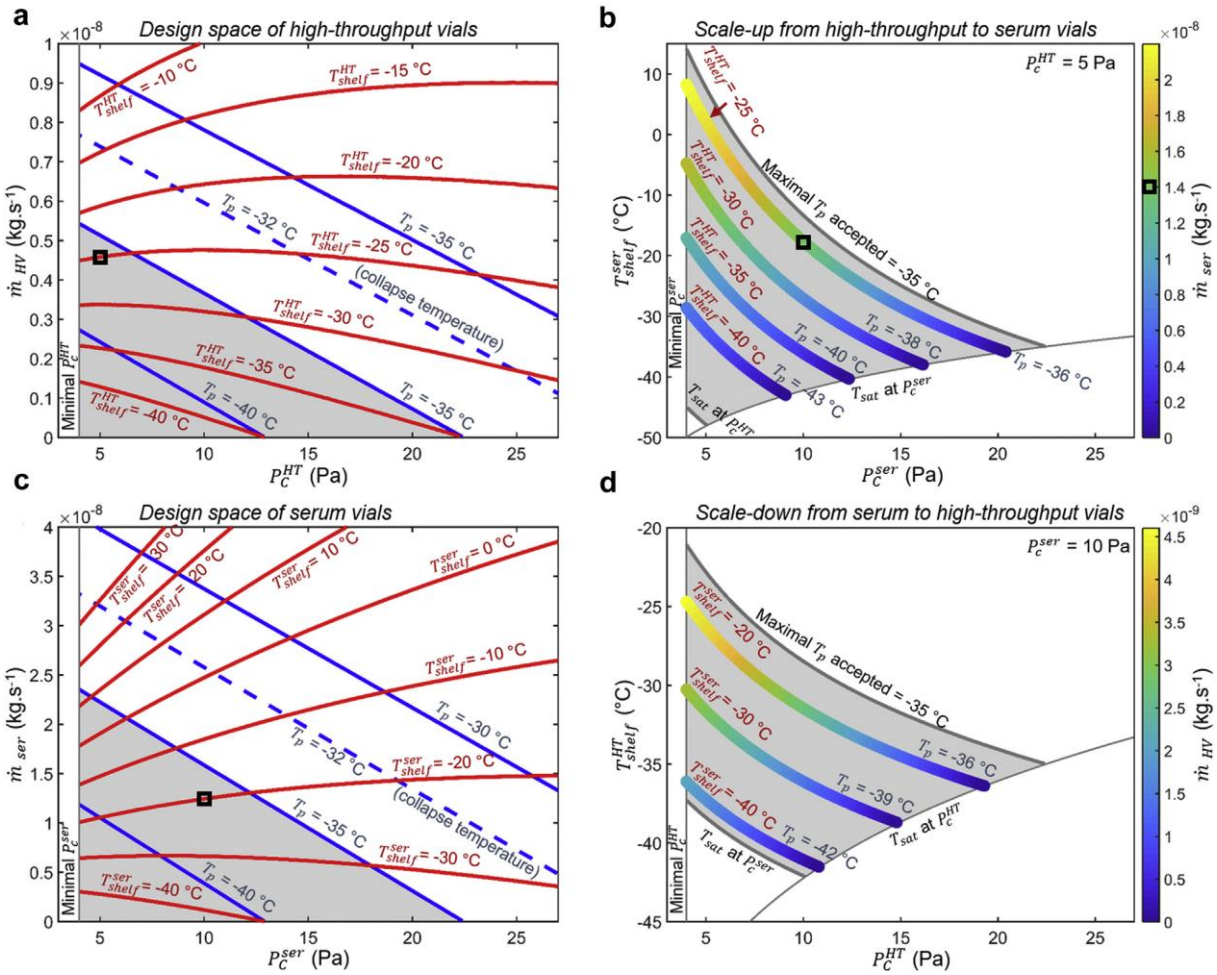

Figure 8 – Primary drying design spaces of a 5% sucrose solution calculated for: (a) high-throughput vials and (c) serum vials; and graphic solution to operate process change from: (b) high-throughput to serum vials, and (d) from serum to high-throughput vials. P_C^{HT}, T_{shelf}^{HT}, and $\dot{m}_{HV}$ are the chamber pressure, shelf temperature and sublimation mass flow rate during primary drying performed with high-throughput vials, respectively. P_C^{ser}, T_{shelf}^{ser}, and $\dot{m}_{ser}$ are the chamber pressure, shelf temperature and sublimation mass flow rate during primary drying performed with serum vials, respectively. T_{sat} is the ice-vapour equilibrium temperature. T_p is the product temperature, and the maximal T_p considered was -35 °C. Blue lines in Figure 8a and Figure 8c represent iso-T_p curves and red lines iso-T_{shelf} curves. The grey area in the four graphs represents the safe zone of the process where T_p is lower than -35 °C. Linear colour maps in (b) and (d) represent iso-T_p curves. Calculations were performed considering the global heat transfer coefficient between the shelf and the vial bottom for 500-µL vials in A-type well plates.

Table 1 – Well plate, vial dimensions, properties and physical properties used in this study.

Symbol	Significance	Value	Standard deviation	Units	Source
Well plate (A-type and B-type)					
A_{WP}	Bottom area of the well plate	1.08×10^{-2}	-	m^2	Calculated
d_{well}	Diameter of the wells	9.2655×10^{-3}	0.0056×10^{-3}	m	Measured
h_{well}	Depth of the wells	1.5245×10^{-2}	-	m	Measured
L_{WP}	Well plate length	1.2712×10^{-1}	-	m	Measured
W_{WP}	Well plate width	8.519×10^{-2}	-	m	Measured
ε_{WP}	Emissivity of the well plate	0.87	-	Dimensionless	Measured
High-throughput vial					
A_{HV}	Outer bottom area of the vial	6.103×10^{-5}	0.039×10^{-5}	m^2	Calculated
A_{in}^{HV}	Inner bottom area of the vial	4.081×10^{-5}	0.032×10^{-5}	m^2	Calculated
A_C^{HV}	Vial-well plate contact area	1.93×10^{-5}	0.71×10^{-5}	m^2	Measured
d_{VE}	Outer bottom diameter of the vial	8.815×10^{-3}	0.028×10^{-3}	m	Measured
d_{VI}	Inner bottom diameter of the vial	7.208×10^{-3}	0.028×10^{-3}	m	Measured
$h_{HV,500}$	500-µL vial height	1.569×10^{-2}	0.0066×10^{-2}	m	Measured
$h_{HV,1000}$	1000-µL vial height	2.906×10^{-2}	0.0083×10^{-2}	m	Measured
l_{HV}^{max}	Maximum bottom concavity	9.0×10^{-5}	1.9×10^{-5}	m	Measured
l_{HV}^{min}	Minimum bottom concavity	4.4×10^{-5}	2.3×10^{-5}	m	Measured
ε_{HV}	Emissivity of the vial	0.85	-	Dimensionless	Measured
Serum vial					
A_V^{ser}	Outer bottom area of the vial	2.07×10^{-4}	0.37×10^{-4}	m^2	(Scutellà et al., 2017a)
A_i^{ser}	Inner bottom area of the vial	1.78×10^{-4}	0.29×10^{-4}	m^2	(Scutellà et al., 2017a)
A_C^{ser}	Vial-shelf contact area	1.67×10^{-5}	0.40×10^{-5}	m^2	(Scutellà et al., 2017a)
l_V^{ser}	Mean bottom curvature depth	1.23×10^{-4}	0.34×10^{-4}	m	(Scutellà et al., 2017a)
k_{ser}^{cc}	Empirical constant for serum vial-shelf contact conduction	2.20×10^{5}	0.27×10^{5}	$W.m^{-4}.K^{-1}$	(Scutellà et al., 2017a)
ε_V	Emissivity of the vial	0.78	-	Dimensionless	(Scutellà et al., 2017a)
Other parameters					
F_{HV}	Visualisation factor at the bottom of the vial [equation (21)]	0.75	-	Dimensionless	Calculated
F_{WP}	Visualisation factor at the bottom of the well plate [equation (22)]	0.18	-	Dimensionless	Calculated
L_{ice}	Initial ice thickness				

	In 500-µL vial	9.8×10^{-3}	-	mm	Calculated
	In 1000-µL vial	1.5×10^{-2}	-	mm	Calculated
P_t	Triple point pressure of water	611.66	-	Pa	(Wagner et al., 1994)
R	Ideal gas constant	8.3144	-	$J.K^{-1}.mol^{-1}$	Perry and Green, 2008)
R_P	Area-normalized product resistance	1.248×10^{5}	-	$Pa.s.m^2.kg^{-1}$	(Konstantinidis et al., 2011)
T_t	Triple point temperature of water	273.16	-	K	(Perry and Green, 2008)
ΔH_{sub}	Mass latent heat of sublimation of ice	2.763×10^{6}	-	$J.kg^{-1}$	(Scutellà et al., 2017a)
$\widetilde{\Delta H_{sub}}$	Molar latent heat of sublimation of ice	5.1059×10^{4}	-	$J.mol^{-1}$	(Murphy and Koop, 2005)
ε_{shelf}	Emissivity of the shelf	0.18	-	Dimensionless	Measured
λ_{gas}^{cont}	Thermal conductivity of the water vapour at atmospheric pressure	0.025	-	$W.m^{-1}.K^{-1}$	(Haynes, 2014)
λ_{ice}	Thermal conductivity of the ice	2.23	-	$W.m^{-1}.K^{-1}$	(Scutellà et al., 2017a)
Λ_0	Free molecular flow heat conductivity	1.99	-	$W.m^{-2}.K^{-1}.Pa^{-1}$	(Pikal, 2000)
σ	Stefan-Boltzmann constant	5.67×10^{8}		$W.m^{-2}.K^{-4}$	(Perry and Green, 2008)

Table 2 – Heat transfer model coefficients evaluated by fitting equation (25) to K_V data obtained in 500-µL and 1000-µL high-throughput vials in A-type and B-type well plates, as well as coefficients for serum vials taken from Scutellà et al. (2017a).

	$K_V^{cc}+K_V^{rad}$ (W m^{-2} K^{-1})	α_V	l_V (m)
A-type – 500-µL	11.23 ± 0.40	0.884 ± 0.036	(3.460 ± 0.067) ×10^{-4}
A-type – 1000-µL	4.7 ± 1.2	2.15 ± 0.17	(3.375 ± 0.044) ×10^{-4}
B-type – 500-µL	14.34 ± 0.92	0.822 ± 0.062	(1.57 ± 0.14) ×10^{-4}
B-type – 1000-µL	10.77 ± 0.87	1.742 ± 0.092	(2.532 ± 0.040) ×10^{-4}
Serum vials (Scutellà et al., 2017a)	4.22 ± 0.45	0.335 ± 0.013	(1.23 ± 0.34) ×10^{-4}

Mean values ± standard errors. $K_V^{cc}+K_V^{rad}$ is the pressure-independent contribution to heat transfer by contact conduction and radiation, α_V is the effective thermal accommodation coefficient, and l_V is the effective distance between surfaces for the gas conduction contribution.

Table 3 – Heat transfer model coefficients calculated or fitted using equations (16), (17) and (19) to (24) to K_{WP} and K_{HV} data obtained in 500-µL and 1000-µL high-throughput vials in A-type and B-type well plates.

	K^{rad} (W.m^{-2}.K^{-1})	K^{cc} (W.m^{-2}.K^{-1})	α	l (m)
K_{WP}				
A-type	0.601 ± 0.038	2.91 ± 0.93	0.813 ± 0.074	(3.28 ± 0.16) ×10^{-4}
B-type	0.601 ± 0.038	3.58 ± 0.60	0.848 ± 0.043	(2.405 ± 0.087) ×10^{-4}
K_{HV}				
A-type – 500-µL	2.20 ± 0.29	96.4 ± 1.0	0.32 ± 0.019	(6.7 ± 0.7) ×10^{-5}
A-type – 1000-µL	2.20 ± 0.29	200.0 ± 3.6	0.024 ± 0.058	(6.7 ± 0.7) ×10^{-5}
B-type – 500-µL	2.20 ± 0.29	172.4 ± 4.7	0.686 ± 0.094	(6.7 ± 0.7) ×10^{-5}
B-type – 1000-µL	2.20 ± 0.29	252.5 ± 8.4	1.23 ± 0.20	(6.7 ± 0.7) ×10^{-5}

Mean values ± standard errors. K_{WP} and K_{HV} are the heat transfer coefficients between the shelf and the well plate bottom, and the well plate bottom and the vial bottom, respectively. K^{rad} is the contribution to K_{WP} or K_{HV} due to heat transfer by the calculated radiation, K^{cc} is the fitted contribution to K_{WP} or K_{HV} due to heat transfer by contact conduction, α is the fitted thermal accommodation coefficient for gas conduction in K_{WP} or K_{HV}, and l is the effective distance between the shelf and well plate surfaces or between the well plate and the vial.